

Pseudo-Orthogonal Chirp-Based Multiple Ultrasonic Transducer Positioning

Mohammad Omar Khyam, Shuzhi Sam Ge, *Fellow, IEEE*, Xinde Li, *Senior Member, IEEE*,
and Mark R. Pickering, *Member, IEEE*

Abstract—Distance-based ultrasonic positioning systems (UPSS) using the trilateration algorithm have been adopted in various types of applications across a wide variety of fields. Recently, the use of a chirp signal in conjunction with cross-correlation has drawn a considerable amount of attention for UPSS. However, when they use a chirp signal for positioning, they suffer from the multiple-access problem due to signal interference. In this paper, to solve this problem, we propose two sets of pseudo-orthogonal chirp waveforms. The basic idea behind the first one is to exploit the orthogonality of the sub-carriers of a chirp waveform, i.e., the discrete frequency components of a chirp waveform, whereas the second one not only exploits the orthogonality of the sub-carriers of a chirp waveform but also chirp rates as a mechanism for assigning uniquely modulated chirp signals to the transmitters. All the waveforms contained in each set have good orthogonality and all the advantages of a classic chirp waveform. First, the performances of the waveforms are investigated through correlation analysis and then, in an indoor environment, evaluated through simulations and experiments for ultrasonic positioning.

Index Terms—Multiple-access, time-of-flight, pseudo-orthogonal chirp waveforms, ultrasonic indoor positioning.

I. INTRODUCTION

THE location of an US transducer can be determined in three-dimensional (3D) space using information regarding its distances from at least three reference points, the locations of which are known, providing that the configuration of these reference points is adequate [1]. This technique has been extensively used in research and production fields for many and varied applications, such as indoor positioning, [2]–[8], robotic navigation [9], [10] and human pose estimation [11].

The process for obtaining distance information is begun by sending an US burst through the air from a transmitter to a receiver, with its traveling time, i.e., time-of-flight (TOF) (t_k),

Manuscript received April 13, 2017; accepted April 15, 2017. Date of publication April 27, 2017; date of current version May 22, 2017. The associate editor coordinating the review of this paper and approving it for publication was Prof. Kazuaki Sawada. (Corresponding author: Mohammad Omar Khyam.)

M. O. Khyam and S. S. Ge are with the Department of Electrical and Computer Engineering, Faculty of Engineering, National University of Singapore, Singapore 117580 (e-mail: fahadete@yahoo.com; samge@nus.edu.sg).

X. Li is with the Key Laboratory of Measurement and Control of CSE, School of Automation, Ministry of Education, Southeast University, Nanjing 210096, China, and also with the Department of Electrical and Computer Engineering, National University of Singapore, Singapore 117580 (e-mail: xindeli@seu.edu.cn).

M. R. Pickering is with the School of Engineering and Information Technology, University of New South Wales, Sydney, NSW 2052, Australia (e-mail: m.pickering@adfa.edu.au).

Digital Object Identifier 10.1109/JSEN.2017.2698470

used to determine the distance (d) between the transmitter and receiver using the common, straightforward law [12]:

$$d = vt_k \quad (1)$$

where v is the speed of sound. In order to accurately estimate the parameter t_k , the transmitter and receiver involved in ranging need to synchronize their local clocks to a common time-scale. Depending on the system's synchronicity, the measured ranges are combined with trilateration or multilateration algorithm to estimate the 3-D position of the target [13].

The position of a target in three-dimensional (3D) space can be determined by measuring its distance (d) from at least three reference points the locations of which are known, providing that the reference points are placed in a single plane non-collinearly i.e., reference points that do not all lie on a single line). Corner points of a equilateral triangle can be considered as an example of such setup. The distance from the target to each reference point is taken as the radius of a sphere centered at that reference point. These spheres will intersect at just two points. One of these intersecting points can usually be discarded as it is located in a physically impossible position (e.g. below the ground or outside the room) so the remaining intersecting point is taken as the position of the target. This process is known as trilateration. Whenever possible, to improve the trilateration's accuracy, more than three reference points are used for coordinate calculation of the target [14], [15]. When more than three reference points are used for coordinate calculation of target it is known as multilateration. Mathematically, if we denote the coordinates of the unknown location of the target as (x, y, z) , the i -th sensor as $(x_i, y_i, 0)$ and the range estimate as d_i , then the following set of equations will hold true \forall_i , assuming no range error [14]:

$$d_i^2 = (x_i - x)^2 + (y_i - y)^2 + z_i^2 \quad (2)$$

For each reference node included in the lateration, a corresponding equation is used. When $i > 3$, this set of quadratic equations can be solved by subtracting the last equation from the others one by one which gives a set of linear equations. Subsequently, singular value decomposition (SVD) [16], [17] or an iterative algorithm (e.g. least squares estimation (LSE)) [18] can be used for solving the set.

The standard TOF estimation technique is cross-correlation, in which transmitted and received signals are cross-correlated

to produce the maximum value at the time delay. It is considered the optimal TOF estimation technique as it uses all the information contained in the signals [19]. However, it performs poorly for estimating the TOF of a single-tone signal because as, in a particular signal length, there are several cycles which produce very similar peaks adjacent to the main one, when the transmitted signal is cross-correlated with the received one, false peaks may be detected in a noisy environment [1], [20]. Although greater cross-correlation accuracy has been achieved by encoding and modulating the single-tone signal with phase shift keying (PSK) [21], its performance degrades in time-varying fading channels [22], [23]. Cross-correlation provides improved accuracy when the waveform is not a single-tone signal but a frequency-modulated (FM) one, such as a linear chirp [20], [22], [24], [25], because it produces a narrower cross-correlated peak at the time delay for a chirp signal.

Therefore, as a chirp-based cross-correlation technique provides more accurate distance estimations through TOF measurements, it has been extensively used in UPSs. However, due to multiple-access interference (MAI), existing chirp-based UPSs suffer from the multiple-access problem [2], [6], [26]–[35], for example, if the useful frequency range of an UPS is 35 kHz to 45 kHz and multiple transmitters transmit the same band of signals simultaneously, they will interfere with each other at the receiving end. Therefore, to support multiple-access in a chirp-based UPS, transmissions of the chirp signals must be orthogonal which can be achieved using either time-division multiplexing (TDM) or frequency-division multiplexing (FDM). In the TDM technique, orthogonality is maintained by transmitting the same pulse from collocated transmitters at different times, i.e., one after another, with proper intervals between them to avoid signal interference at the receiving end. However, as this leads to a slower update rate because only one transmitter is allowed to send at a time, the number of location updates possible in a given time interval is limited [36], [37]. Therefore, this is not an efficient solution for applications for which simultaneous transmission is a prerequisite. In the FDM technique, orthogonality is maintained by ensuring that separate sources are spaced sufficiently far apart in the frequency domain so that no interference occurs, i.e., the bandwidth to the transmitters is split. However, this deteriorates the cross-correlation performance, the accuracy of which depends on the bandwidth of the chirp [20].

Some methods such as direct sequence spread spectrum (DSSS) [5], code division multiple access (CDMA) [4] and frequency hopped spread spectrum (FHSS) [3] have been proposed using broadband transducers that are more expensive than narrowband transducers. A summary of the broadband UPSs can be found in [7], [8]. Please note that as in this paper we proposed multiple access chirp-based ultrasonic positioning, here we only described similar systems and to the best of our knowledge, only one previous paper [30] has demonstrated the use of pseudo-orthogonal chirp waveforms for UPS. This system adapted the use of chirp rates as a mechanism for assigning uniquely modulated chirp signals to transmitters from wireless data communications [38] to

UPS application. As it uses the diversity of the chirp rates for multiple access in an UPS, all the advantages of the classical chirp waveform are present in the system. However, the problem of this approach is that due to the symmetricity of the chirp rate, when the number of transmitters in the system is increased the multiple-access interference (MAI) is also increased. For the ease of discussion and representation, we named this category of chirp set 1 throughout the paper.

In this paper, to solve the multiple-access problem, we propose using two sets of pseudo-orthogonal chirp waveforms which we named set 2 and set 3 respectively. The basic idea behind the set 2 is to exploit the orthogonality of the sub-carriers of a chirp waveform i.e., discrete frequency components of a chirp waveform which we have adapted from the fields of radar communications [39] to the US positioning. In this category of orthogonal chirps (i.e., set 2) when the number of transmitters is increased, the computational cost is also increased. On the other hand, set 3 not only exploits the orthogonality of the sub-carriers of a chirp waveform but also chirp rates as a mechanism for assigning uniquely modulated chirp signals to transmitters. Thus, this category of pseudo-orthogonal chirps (i.e., set 3) provides a satisfactory tradeoff between the computational cost and positioning accuracy i.e., between sets 1 and 2. A detailed discussion, simulation and experimental demonstration of the performances of sets 1 to 3 are presented in this paper.

The rest of this paper is organized as follows: Section II provides a mathematical model which shows how an UPS suffers from the multiple-access problem; in Section III, two sets of pseudo-orthogonal chirp waveforms are presented along with the existing one as solutions to the US multiple access problem; in Section IV, a correlation analysis of each set of pseudo-orthogonal chirp waveforms is presented; in Section V, an assessment of each set of pseudo-orthogonal chirp waveforms scheme in the field of UPSs is demonstrated through simulations; Section VI describes the experimental procedure for determining the accuracy of the pseudo-orthogonal chirp waveforms for sets 1 to 3 for US positioning; the results obtained from the experiments are presented in Section VII; and Section VIII discusses the conclusions drawn from this study and the future research directions.

II. DESCRIPTION OF PROBLEM

If an UPS has M transmitters located at unknown positions which simultaneously transmit a signal ($s_i(t)$, $i = 1, 2, \dots, M$), the signal received by a receiver in the system is [13]:

$$r(t) = \sum_{i=1}^M A_i \cdot (h_i * s_i)(t - t_i) + \tilde{n}(t) \quad (3)$$

where A_i and t_i are the respective amplitude and propagation delay (TOF) of the signal arriving from the i th transmitter and $\tilde{n}(t)$ the additive white Gaussian noise (AWGN), with the convolution operator (*) denoting the filtering effect produced by the US channel's unknown impulse response ($h_i(t)$).

This ideal propagation model takes into account only the direct-path signal. However as, in an indoor environment,

a receiver receives multiple delayed and attenuated replicas of a transmitted signal due to reflections from multiple objects in that environment, the impulse response of the i th transmitter can be modeled as:

$$A_i \cdot (h_i * s_i)(t) \simeq \sum_{l=1}^{L_i} \hat{A}_{il} s_i(t - t_l') \quad (4)$$

where L_i represents the number of copies of the transmitted signal ($s_i(t)$).

The received signal ($r(t)$) is processed using a matched filter implemented by correlating it with a reference signal ($s_k(t)$) (i.e., a locally stored copy of the original emitted signal) which results in:

$$\begin{aligned} c_k(t) &= [r(t) * s_k(t)] \\ &= \left(\sum_{i=1}^M A_i \cdot (h_i * s_i)(t - t_i) + \tilde{n}(t) \right) * s_k(t) \\ &= (A_k \cdot (h_k * s_k)(t - t_k)) * s_k(t) \\ &\quad + \left(\sum_{i \neq k} A_i \cdot (h_i * s_i)(t - t_i) \right) * s_k(t) + \tilde{n}(t) * s_k(t) \end{aligned} \quad (5)$$

In equation (5), the first term on the right-hand side is the auto-correlation of the transmitted signal with itself which is distorted by the channel response ($h_i(t)$), and the second term represents the MAI from all the other transmitters simultaneously transmitting in the environment which are treated by $c_k(t)$ as noise because it follows a single-user approach.

Therefore, the earliest component of $c_k(t)$ is $[s_k * s_k](t - t_k)$ (where $*$ implies a correlation) the peak of which can be used to determine t_k (the direct-path signal of $s_k(t)$) with considerable precision provided the other multipath components (from $s_k(t)$) of $r(t)$ are sufficiently weak and separated in time from $t = t_k$. The MAI and noise (respectively, the second and third terms of equation (5)) may shift the peak at t_k from its actual timeline which could result in an inaccurate estimate of the range information.

Therefore, as MAI has a large effect on the accuracy of TOF estimations, it is often desirable that the cross-correlation between transmitted signals (the second term in equation (5)) is as low as possible. In this paper, we present two sets of pseudo-orthogonal chirp waveforms (i.e., set 2 and set 3) and compare with existing pseudo-orthogonal chirp-based UPS (i.e., set 1). The waveforms contained each set are pseudo-orthogonal. In addition, all the waveforms contained in each set have all the advantages of classic chirp waveform. The basic idea behind the proposed first one is to exploit the orthogonality of the sub-carriers of a chirp waveform i.e., discrete frequency components of a chirp waveform while the second one not only exploits the orthogonality of the sub-carriers of a chirp waveform but also chirp rates as a mechanism for assigning uniquely modulated chirp signals to transmitters. To the best of our knowledge, only one previous paper [30] has demonstrated the use of one kind of pseudo-orthogonal chirp waveforms (which we call set 1 in the entire paper) for UPS. However, it was based on binary data communication and the problem of this approach is that due to the symmetricity of the chirp rates when the number

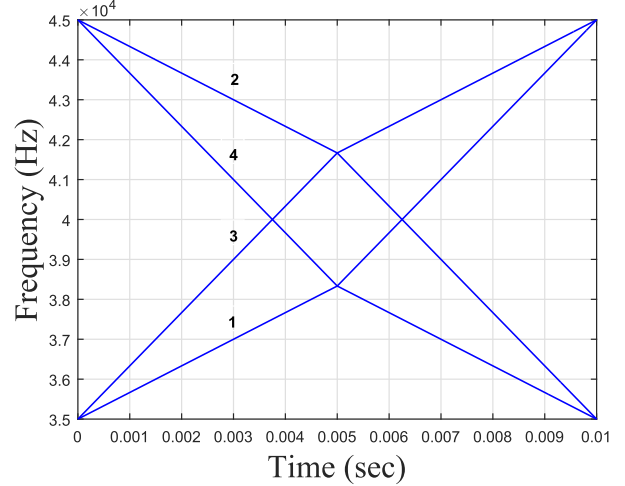


Fig. 1. Illustrations of chirp rates of 35-45 kHz/10 ms chirp waveform for set 1 where each MLC (marked with number 1, 2, 3, and 4) dedicated to the individual transmitter.

of transmitters is increased into the system the MAI is also increased (discussed in Section IV).

III. ULTRASONIC MULTIPLE-ACCESS TECHNIQUES

A. Multi-Linear Chirp Technique for Multiple-Access (Set 1)

A linear chirp is defined as:

$$s(t) = \text{rect}\left[\frac{t}{T_c}\right] \exp\left\{j2\pi\left(f_s t \pm \frac{1}{2}\mu t^2\right) + \phi\right\} \quad 0 \leq t \leq T_c \quad (6)$$

where $\text{rect}(\bullet)$ is a rectangular window function, f_s the starting frequency, T_c the chirp duration, the \pm term defines the sweep direction, ϕ the initial phase, $\mu = \frac{B}{T_c}$ the chirp rate (where bandwidth $B = f_e - f_s$ with f_s and f_e the starting and ending frequencies respectively of the chirp signal) that describes rate of change in frequency as a function of time.

Unlike the single-tone signal, the chirp-rate provides an additional degree of freedom for modulation. Utilizing this parameter in [38] a solution to multiple-access in data communication has been provided where chirp rates are used as a mechanism for assigning uniquely modulated chirp waveforms to the transmitters. As this approach decomposes each chirp into two interconnected linear chirps with different chirp rates that change at the halfway point of the signal, it is called multi-linear chirp (MLC). As a solution to MAI in UPS, [30] used the MLC technique as it has been demonstrated that waveforms occupying the same frequency band but with inverse as well as significantly different chirp rates offer a satisfactory tradeoff between the use of frequency spectra and the performance of cross-correlation suppression. However, it was based on binary data communication and the problem of this approach is that due to the symmetricity of the chirp rates when the number of transmitters is increased into the system the MAI is also increased (discussed in Section IV). The time-frequency diagram of the MLC technique is illustrated in Fig. 1 where each rate represents a different signal waveform that is correlated with the received signal to extract

the TOF information. Mathematically, the above MLC can be uniformly expressed as follows.

Suppose that the waveform duration is T_c , the bandwidth B and phase $\phi = 0$. Then, the M number of waveforms can be uniformly expressed as:

$$\begin{aligned} s_i(t) &= \text{rect}\left[\frac{t}{T_{c_p}}\right] \exp\left\{j2\pi\left(f_{s_p} t \pm \frac{1}{2}\mu_{m_p} t^2\right)\right\} \\ &+ \text{rect}\left[\frac{t - T_{c_p}}{T_{c_q}}\right] \\ &\times \exp\left\{j2\pi\left(f_{s_{iq}}(t - T_{c_p}) \pm \frac{1}{2}\mu_{m_q}(t - T_{c_p})^2\right)\right\} \quad (7) \end{aligned}$$

where the \pm term defines the sweep direction. Using equation (7) one can generate $i = 1, \dots, M$ number of pseudo-orthogonal waveforms by setting $m = 1, \dots, \frac{M}{2}$ as for each m one can generate two pseudo-orthogonal chirp waveforms utilizing the sweep direction.

For positive and negative sweep directions the starting frequencies and chirp rates are expressed respectively by equations (8) and (9) as follows.

$$\begin{aligned} f_{s_p} &= f_l \quad f_{s_{mq}} = f_l + \frac{mB}{M+1} \quad \mu_{m_p} = \frac{m2\mu}{M+1} \\ \mu_{m_q} &= 2\mu - \mu_{m_p} \end{aligned} \quad (8)$$

$$\begin{aligned} f_{s_p} &= f_h \quad f_{s_{mq}} = f_h - \frac{mB}{M+1} \quad \mu_{m_p} = \frac{m2\mu}{M+1} \\ \mu_{m_q} &= 2\mu - \mu_{m_p} \end{aligned} \quad (9)$$

where f_l and f_h are the respective lowest and height frequency of the chirp signal. According to equations (8) and (9) if the number of waveforms (i.e., the number of transmitters) M is increased, the gap between the starting frequency of two chirp waveforms at the half way point will decrease which will increase symmetricity in chirp rates, as a result, the signal interference between the pseudo-orthogonal chirp waveforms will increase i.e., the TOF estimation accuracy will decrease (according to equation (5)). This phenomenon can be visualized in Fig. 1 and further discussed in Section IV.

B. Multiple-Access Using Orthogonality of Discrete-Frequency Components of a Chirp (Set 2)

The fundamental idea behind this technique for simultaneous multiple transducer positioning is to utilize the orthogonality of the discrete frequency components of a chirp waveform.

This technique works in a three-stage process. In the first stage, the fast Fourier transform (FFT) of a chirp signal is placed in the discrete data sequence serially, as shown in Fig. 2 where there are N discrete spectra ($S[1], S[2], \dots, S[N]$). Mathematically, the data sequence of a chirp spectrum (i.e., stage 1) is given by:

$$S[p] = \text{DFT}[s[n]] \quad (10)$$

where $s[n]$ represent the chirp signal in the discrete domain which can be obtained by introducing $t = nT_s$ in equation (6) where $n = 1, 2, \dots, N$ and T_s is the sampling interval.

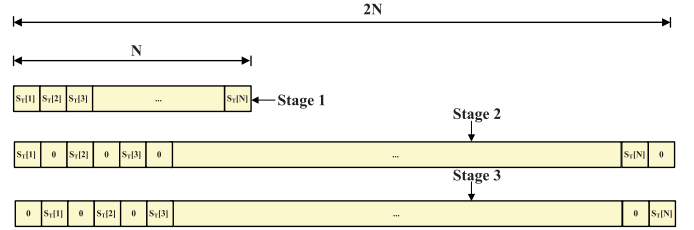


Fig. 2. Illustrations of data sequence of discrete spectra allocated to transmitters for set 2

As the second stage involves interleaving $M - 1$ zeros after each discrete spectrum, where M represents the number of transmitters used by an UPS, the new data sequence has MN discrete spectra, with the data sequence obtained dedicated to the first transmitter. Based on the example shown in Fig. 2, if two transmitters are used by an UPS, we need to insert one ($M - 1 = 2 - 1 = 1$) zero after each discrete spectrum. It is noted that, due to its zero interleaving, the length of the data sequence is increased from N to $2N$ (i.e., $MN = 2N$). In addition, it (zero interleaving) refers to the repetition of the signal (M times). Mathematically, in the time-domain, the signal dedicated to the first transmitter (i.e., the time domain signal of stage 2) is defined as:

$$\begin{aligned} s_1(t) &= s(t)\text{rect}\left(\frac{t}{T_c}\right) + s(t - T_c)\text{rect}\left(\frac{t - T_c}{T_c}\right) \\ &+ \dots + s(t - (M - 1)T_c)\text{rect}\left(\frac{t - (M - 1)T_c}{T_c}\right) \end{aligned} \quad (11)$$

In the third stage, the data sequence obtained in the second stage is shifted by $i = 1, \dots, M - 1$ (i.e., shift the DFT profiles by $\frac{i}{MT_c}$ in frequency) to generate the remaining data sequences which are dedicated to the rest of the transmitters used by the UPS; for example, in Fig. 2, the data sequence obtained from the second stage is initially shifted by one and then two to generate the other two data sequences. Since the DFT profiles are shifted $\frac{i}{MT_c}$ in frequency, mathematically, in the time-domain, the signal dedicated to the remaining transmitters (i.e., time domain signals of stage 3) is defined as:

$$s_{(i+1)}(t) = s_1(t)e^{(j2\pi\frac{i}{MT_c}t)} \quad (12)$$

Although all these signals are transmitted in parallel from individual transmitters, the receivers receive them without any interference as the multiplication of their respective spectra results in zero which means they are orthogonal, as shown in Fig. 2 for three chirp signals.

According to equation (12), if i is increased, the number of orthogonal chirps will increase which will increase system capacity, however, at the same time, based on equation (11), the length of each waveform will increase M times which will increase the processing time and system cost. For example, to generate four chirp signals (i.e., $M = 4$) (which do not interfere with each other) from a 10 ms duration of a 35-45 kHz linear chirp (defined in equation (6)), the length of each chirp waveform will become 40 ms according to equation (11).

C. Hybrid Technique (Set 3)

Set 1 that uses the diversity of the chirp rates for multiple-access, the error in TOF estimation is proportional to the scalability i.e., if the number of transmitters is increased the error in TOF estimation will increase. On the other hand, set 2 that exploits the orthogonality of the sub-carriers of a chirp waveform for multiple-access, the computational complexity is proportional to the scalability i.e., if the number of transmitters is increased the signal length will increase. Therefore, to overcome the problems of set 1 and set 2 (i.e., accuracy and computational cost respectively), we propose to combine both techniques to provide a satisfactory tradeoff between the accuracy and computational cost. And it can be obtained by replacing the linear chirp in equation (11) (by setting $M = 2$) with a pair of MLC described in equations (7) followed by shifting the DFT profiles in frequency as described in equation (12). Mathematically, the whole phenomenon can be described by equations (13)-(14) as follows.

$$\begin{aligned} s_i(t) &= \text{rect}\left(\frac{t}{T_c}\right) \exp\left\{j2\pi\left(f_{s_p} t \pm \frac{1}{2}\mu_{m_p} t^2\right)\right\} \\ &\quad + \text{rect}\left(\frac{t-T_c}{T_c}\right) \\ &\quad \times \exp\left\{j2\pi\left(f_{s_{iq}}(t-T_c) \pm \frac{1}{2}\mu_{m_q}(t-T_c)^2\right)\right\} \end{aligned} \quad (13)$$

$$s_{(i+M/2)}(t) = s_i(t)e^{(j2\pi\frac{i}{2T_c}t)} \quad (14)$$

where the \pm term defines the sweep direction. For positive and negative sweep directions the starting frequencies and chirp rates are expressed respectively by equations (8) and (9) where $m = 1, \dots, \frac{M}{4}$.

For set 3 using equations (13)-(14) we can generate M number of waveforms utilizing $\frac{M}{2}$ number of MLC components (because for set 3 $m = 1, \dots, \frac{M}{4}$) whereas to generate M number of waveforms set 1 requires M number of MLC components (because for set 1 $m = 1, \dots, \frac{M}{2}$). Therefore, the TOF estimation errors for set 3 will be reduced to half when compared to set 1 although for set 3 each signal length will be increased from M to $2M$ (according to equations (13)-(14)). At the same time, for set 3 (in equations (13)-(14)) we can generate M number of waveforms using a signal length of $2T_c$ whereas to generate M number of waveforms set 2 requires a signal length of MT_c . Therefore, for $M > 2$ the computational complexity of set 3 will be reduced to half when compared to set 2 although the accuracy for set 2 will be lower as it uses $\frac{M}{2}$ number of MLC components whereas set 1 use only use a linear chirp. Thus, a satisfactory tradeoff between the computational cost and accuracy for an US multiple-access system has been designed. A more detailed analysis can be found in Section IV.

IV. ANALYSIS OF WAVEFORM PERFORMANCE

For multiple-access, an important property is the relative difference between the auto-correlations of identical waveforms and cross-correlations of different ones which we now investigate for each set of chirp waveforms described in earlier section. During these performance evaluations, we use

$f_l = 35$ kHz, $f_h = 45$ kHz, $T_c = 10$ ms, $T_s = 1$ μ s, and $M = 4$.

For the first, second, and third sets of pseudo-orthogonal chirp waveforms described in Section III, the relative differences between the auto-correlations of identical waveforms and cross-correlations of different ones are shown in Fig. 3, Fig. 4 and Fig. 5 respectively.

For the waveforms contained in set 1, compared with the auto-correlations, the suppression of cross-correlations between $s_1(t)$, $s_2(t)$, $s_1(t)$, $s_4(t)$; $s_2(t)$, $s_3(t)$; and $s_3(t)$, $s_4(t)$ (shown in Fig. 3(a),(c),(d) and (f) respectively) is higher than that between $s_1(t)$, $s_3(t)$ and $s_2(t)$, $s_4(t)$ (shown in Fig. 3(b) and (e) respectively). This is because $s_1(t)$, $s_2(t)$ and $s_3(t)$, $s_4(t)$ used completely opposite chirp rates i.e., asymmetric chirp rates (shown in Fig 1) whereas $s_2(t)$, $s_4(t)$ used same directional chirp rates i.e., symmetric chirp rates (shown in Fig. 1). Intensely, compared with the auto-correlations, the suppression of cross-correlations between $s_1(t)$, $s_2(t)$ and $s_3(t)$, $s_4(t)$ (shown in Fig. 3(a) and (f) respectively) is slightly higher than that between $s_1(t)$, $s_4(t)$ and $s_2(t)$, $s_3(t)$ (shown in Fig. 3(c) and (d) respectively). This is because $s_1(t)$, $s_2(t)$ and $s_3(t)$, $s_4(t)$ used completely opposite chirp rates as discussed earlier (shown in Fig. 1) whereas although $s_1(t)$, $s_4(t)$ and; $s_2(t)$, $s_3(t)$ used opposite chirp rates, they are slightly symmetric (shown in Fig. 1).

For the waveforms contained in set 2, the relative differences between the auto-correlations of the identical waveforms and cross-correlations of different ones are shown in Fig. 4. It can be seen that due to its repetition property, the auto-correlations of all waveforms produce multiple peaks while the cross-correlations are fully suppressed in a central window around the zero-shift (as the spectral components of $s_1(t)$, $s_2(t)$, $s_3(t)$ and $s_4(t)$ are mutually shifted by $\frac{1}{4T_c}$ according to equation (12)) with large side peaks out of this window (due to the signal's repetition property) which makes the waveforms pseudo-orthogonal. Please note that here to generate four pseudo-orthogonal chirp waveforms, it was required to use signal length of $4T_c = 40$ ms whereas it was $T_c = 10$ ms for set 1.

For the waveforms contained in set 3, the relative differences between the auto-correlations of the identical waveforms and cross-correlations of different ones are shown in Fig. 5. It can be seen that due to the signal's repetition property, the auto-correlations of all waveforms produce multiple peaks while the cross-correlations suppression varies with waveform's characteristics. For $s_1(t)$, $s_3(t)$ and $s_2(t)$, $s_4(t)$ the cross-correlations are fully suppressed in a central window around the zero-shift with large side peaks out of this window which makes the waveforms pseudo-orthogonal (shown in Fig. 5(b) and (e) respectively). This is because the DFT profiles of $s_1(t)$, $s_2(t)$ and $s_3(t)$, $s_4(t)$ are shifted $\frac{1}{2T_c}$ in frequency relative to one another. For $s_1(t)$, $s_4(t)$ and $s_2(t)$, $s_3(t)$ the cross-correlations are fully suppressed all over the window (i.e., no side peaks) because the DFT profiles of $s_1(t)$, $s_4(t)$ and $s_2(t)$, $s_3(t)$ are not only shifted $\frac{1}{2T_c}$ in frequency relative to one another but also use completely opposite chirp rates. On the other hand, for $s_1(t)$, $s_2(t)$ and $s_3(t)$, $s_4(t)$ although the cross-correlations are fully suppressed

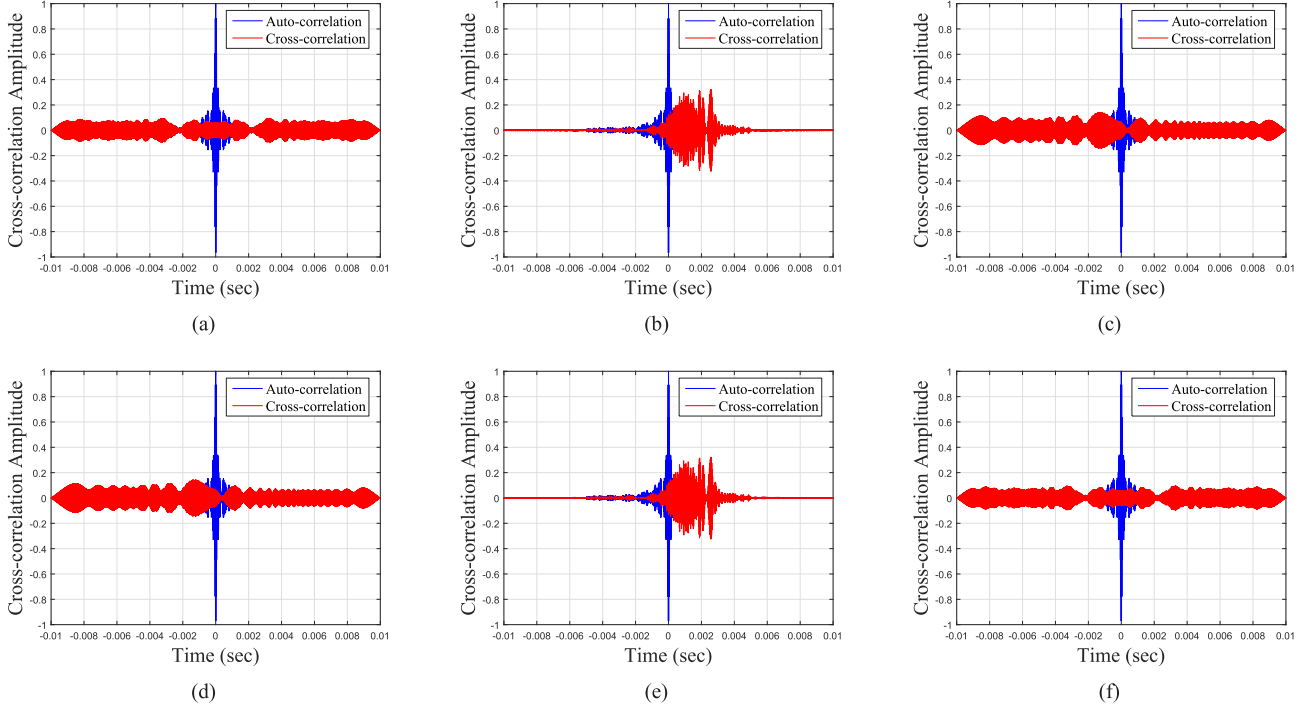


Fig. 3. Comparisons of auto-correlations and cross-correlations of three waveforms for set 1: (a) waveforms 1 and 2; (b) waveforms 1 and 3; (c) waveforms 1 and 4; (d) waveforms 2 and 3; (e) waveforms 2 and 4; and (f) waveforms 3 and 4.

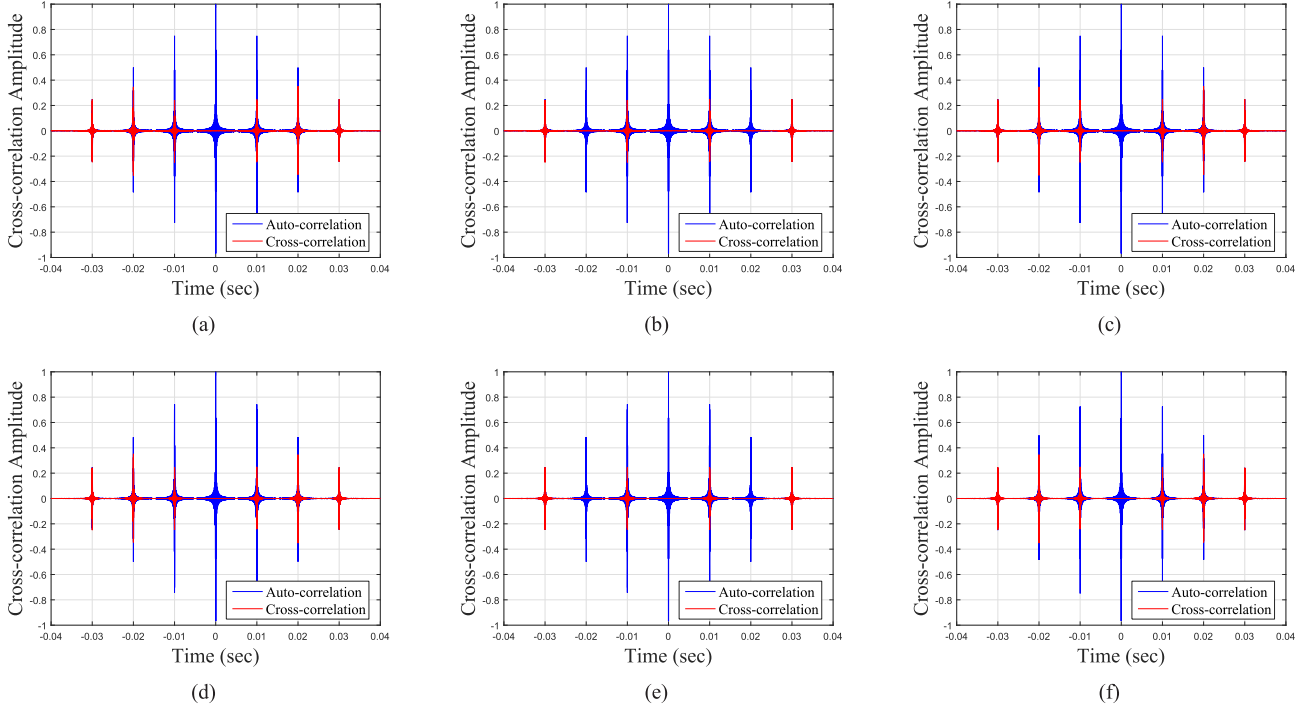


Fig. 4. Comparisons of auto-correlations and cross-correlations of three waveforms for set 2: (a) waveforms 1 and 2; (b) waveforms 1 and 3; (c) waveforms 1 and 4; (d) waveforms 2 and 3; (e) waveforms 2 and 4; and (f) waveforms 3 and 4.

all over the window (i.e., no side peaks), at the center the suppression is slightly lower when compared to $s_1(t)$, $s_4(t)$ and $s_2(t)$, $s_3(t)$. This is because their (i.e., $s_1(t)$, $s_2(t)$ and $s_3(t)$, $s_4(t)$) DFT profiles are not shifted in frequency relative to one another but, use completely opposite chirp rates. Please note that in this pseudo-orthogonal chirp category, to generate four

pseudo-orthogonal chirp waveforms, it was required to use signal length of $2T_c = 20$ ms whereas it was $4T_c = 40$ ms for set 2.

In summary, according to Figs. 3-5, for set 1 the MAI was higher than other sets, for set 2 although the MAI was lower than other sets, the signal length was higher than other sets

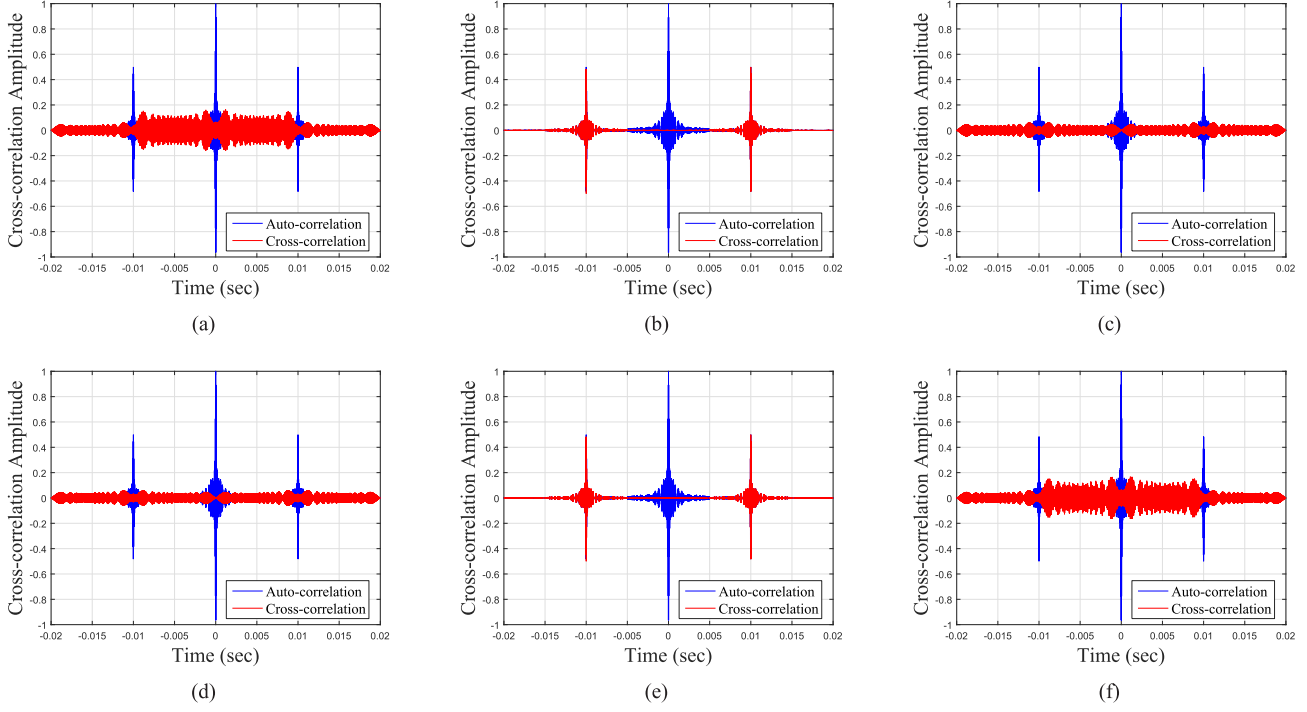


Fig. 5. Comparisons of auto-correlations and cross-correlations of three waveforms for set 3: (a) waveforms 1 and 2; (b) waveforms 1 and 3; (c) waveforms 1 and 4; (d) waveforms 2 and 3; (e) waveforms 2 and 4; and (f) waveforms 3 and 4.

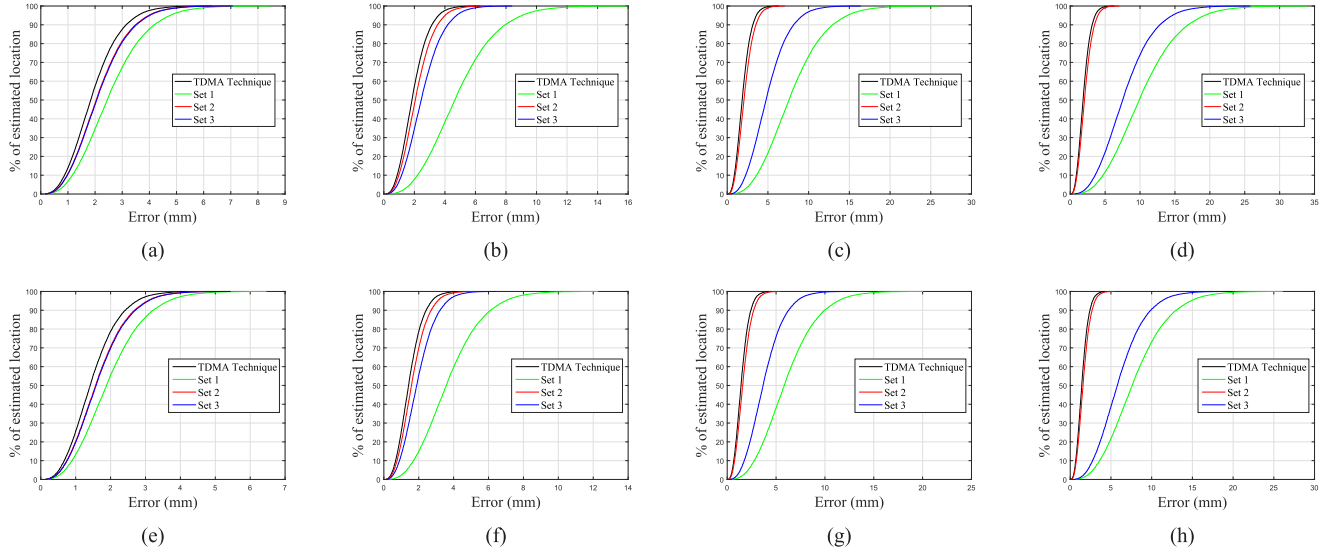


Fig. 6. Cumulative absolute location errors (from simulations) for TDM technique and all sets of pseudo-orthogonal chirp waveforms when number of targets (transmitters) were: (a) 2; (b) 4; (c) 6 and (d) 8 at -5 dB SNR and, (e) 2; (f) 4; (g) 6 and (h) 8 at 0 dB SNR.

and for set 3 a satisfactory tradeoff between the MAI and the signal length was obtained.

It can be seen that, as due to the repetition property presented in sets 2 and 3, there are multiple peaks involve in the correlation process, the peak generated by the reflected path may exceed the main one of $c_k(t)$ (i.e., cross-correlation in equation (5)) due to multipath, MAI and noise, and that associated with the correct delay is not always the highest one. In some cases, the direct path can experience attenuation,

which gives it a lower cross-correlation peak than indirect multi-paths. In other cases, a number of indirect paths can combine to produce a peak that is greater than the one associated with the direct path [40].

Therefore, a threshold-based search mechanism [40] is applied to find the first cross-correlation peak in the second half of the time domain cross-correlation output above the noise floor. The second half of the time-domain cross-correlation output is chosen because the delay in

TABLE I
COORDINATES OF THE 3D RECTANGULAR ROOM, AND IDEAL POSITIONS
OF THE REFERENCE POINTS AND TARGET TRANSDUCER (cm)

	<i>x</i>	<i>y</i>	<i>z</i>
Room (top left corner)	-300	300	0
Room (bottom right corner)	300	0	0
Reference Point 1	-60	60	0
Reference Point 2	60	60	0
Reference Point 3	0	120	0
Target 1	-5	95	100
Target 2	5	95	100
Target 3	-5	90	100
Target 4	5	90	100
Target 5	-5	100	100
Target 6	5	100	100
Target 7	0	90	100
Target 8	0	100	100

the time-domain cross-correlation output always presents at the second half. The earliest peak (in the second half of the time domain cross-correlation output) is assumed to belong to the direct path that gives the correct TOF. In this work, the threshold is set to 70% of the height cross-correlation value as that value is found to be sufficiently high (through simulations and experiments) to detect the earliest peak (in the second half of the time domain cross-correlation output) above the noise floor and sufficiently low to guarantee detection of the direct-path, even with strong reflections.

V. SIMULATION RESULTS

A customized environment was simulated in Matlab to evaluate the performances of the proposed waveform schemes for multiple-access in an UPS. In a virtual 3D rectangular room, in an active mobile architecture, three reference points i.e., receivers (with known locations) were considered and eight transmitters introduced sequentially (two transmitters at a time) with the aim of localizing them, with the true positions of the transmitters known. Please note that although one can introduce eight transmitters sequentially with one transmitter at a time, we introduced two because set 3 can generate two pseudo-orthogonal chirp waveforms from one MLC component as discussed in Section III-C. Table I shows the coordinates (*x*, *y*, *z*) of the room, reference points (receivers), and targets (transmitters). According to the procedure described in Section III, with a sampling rate of 1 Msample/s, three sets of pseudo-orthogonal chirp waveforms were generated, from a 35-45 kHz/10 ms chirp signal and dedicated to the corresponding transmitters. The waveforms contained in sets 1 to 3 were same as the number of transmitters and each waveform was modeled with a 35-45 kHz bandpass filter. The waveforms contained in each set were transmitted simultaneously from the targets (transmitters) and received by the reference points (receivers). The position of each transmitter was calculated using trilateration algorithm described in Section I. The distance information used in the trilateration algorithm was obtained using equation (1) with the TOF (*t_k*) calculated using cross-correlation technique along with the threshold-based earliest correlation peak search mechanism described in Section IV. For the simulation, it was assumed that the channel was subjected to AWGN

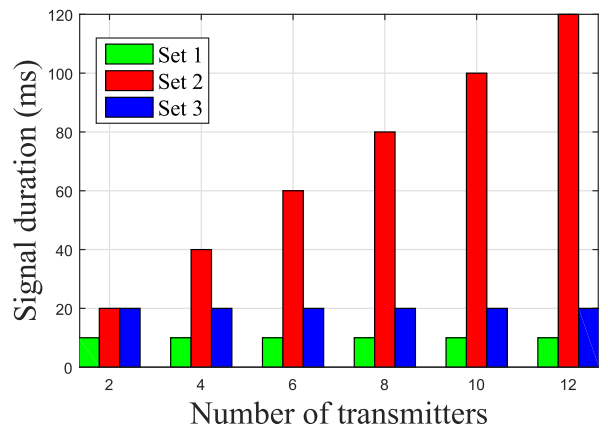


Fig. 7. Effect of number of transmitters on signal length.

with SNR of -5 dB and 0 dB and six multi-paths at random positions with reflection coefficients of 0.7, and each was run for 20000 iterations. Please note that although we considered multipaths at random position, it was ensured that the minimum separation between each path was larger than $\frac{1}{B}$ sec because chirp signals sweeping B Hz can resolve two different chirp signals traversing with $\frac{1}{B}$ sec path difference [22].

To demonstrate the performance of the sets 1 to 3, the positions of the transmitters were also calculated by the TDM technique using 35-45 kHz/10 ms chirp. For the TDM technique, the orthogonality was maintained by transmitting the same pulse from collocated transmitters at different times. The cumulative absolute location errors of the transmitters for each set of pseudo-orthogonal chirp waveforms and TDM techniques are shown in Fig. 6, with the cumulative errors for 90% of cases presented in Table II in which the RMSEs of the absolute location errors of the transmitters are also given. The computational complexity in terms of signal length for each set is shown in Fig. 7. The results indicate that, for the same environment, for each set of pseudo-orthogonal chirp waveforms, the error and computational complexity varied. The error varied depending on the cross-correlation suppression between the pseudo-orthogonal chirp waveforms contained in each set and noise and the computational complexity varied depending on the signal's repetition property. A high or low error means a low or high cross-correlation suppression and a low or high SNR, and a high or low computational complexity means a high or low signal repetition. It is important to note that the results (Fig. 6 and Table II) confirmed that when noise was increasing into the system the error was also increasing which was expected according to equation (5) and discussion provided in Section II. Therefore, for the sake of brevity we limited our analysis for SNR -5 dB and 0 dB which is educate for analyzing an UPS [40].

To visualize the effect of multipath on the repetition property presented in set 2 and 3, an example from this simulation for set 2 is illustrated in Fig. 8 when the SNR was 0 dB, *M* = 4, and the delay between a target (target 1) and a reference point (reference point 1) was 3470 samples which correspond to 119.37 cm when the speed of sound is 344 m/s at 21°C. In this particular case, a number of indirect paths

TABLE II
ABSOLUTE LOCATION ERRORS (FROM SIMULATIONS) OF TARGET OBTAINED FOR TDM TECHNIQUE AND ALL SETS OF PSEUDO-ORTHOGONAL CHIRP WAVEFORMS IN TERMS OF CDF AND RMSE (mm)

Methods	Number of Transmitters															
	2				4				6				8			
	SNR		SNR		SNR		SNR		SNR		SNR		SNR		SNR	
	RMSE	CDF	RMSE	CDF	RMSE	CDF	RMSE	CDF	RMSE	CDF	RMSE	CDF	RMSE	CDF	RMSE	CDF
TDM	2.1383	3.1418	1.6449	2.4168	2.1407	3.1453	1.6467	2.4194	2.1383	3.1418	1.6449	2.4168	2.1360	3.1383	1.6430	2.4141
Set 1	2.8448	4.1798	2.1883	3.2152	5.4051	7.9416	4.1578	6.1089	8.8188	12.9573	6.7837	9.9671	11.4929	16.8863	8.8407	12.9894
Set 2	2.3730	3.4866	1.8254	2.6820	2.3944	3.5180	1.8418	2.7061	2.3944	3.5180	1.8418	2.7061	2.3683	3.4797	1.8218	2.6767
Set 3	2.3944	3.5180	1.8418	2.7061	2.8448	4.1798	2.1883	3.2152	5.5473	8.1506	4.2672	6.2697	8.7335	12.8319	6.7181	9.8707

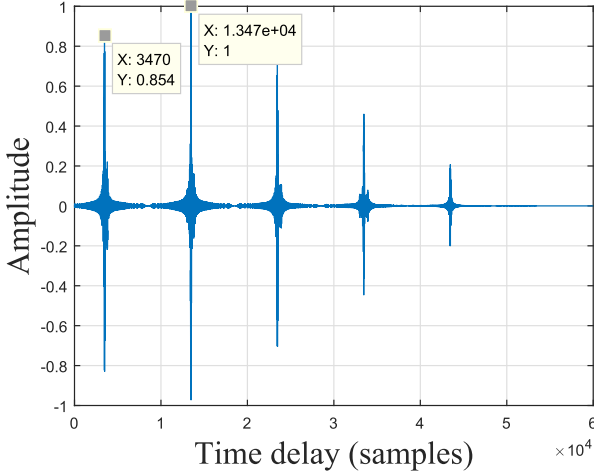


Fig. 8. Visualization of multipath effect when a number of indirect paths combined at such delay where signal repetition occurred.

combined at such delay where signal repetition occurred (that can be seen in Fig. 8 where the delay difference between the marked peaks is 10000 samples i.e., 10 ms which is equal to the original signal length) which produced a peak that is greater than the one associated with the direct path. Therefore, to overcome such kind of error, the threshold-based search mechanism (described in Section IV) was applied to find the earliest arriving cross-correlation peak (in the second half of the time domain cross-correlation output) above the noise floor which was assumed to belong to the direct path that gave the correct TOF. As discussed earlier, the threshold was set to 70% of the height cross-correlation value as that value was found to be sufficiently high to detect the earliest peak (in the second half of the time domain cross-correlation output) above the noise floor and sufficiently low to guarantee detection of the direct-path, even with strong reflections.

VI. EXPERIMENTAL PROCEDURE

To evaluate the performances of the proposed waveform schemes for multiple-access in an UPS, experiments were conducted in indoor noisy and multi-path environments. In an active mobile architecture, three reference points (receivers) with known locations were considered and eight targets (transmitters) introduced sequentially (two transmitters at a time) with the aim of localizing them. Please note that the transmitters were placed on a single plane (i.e., on a board

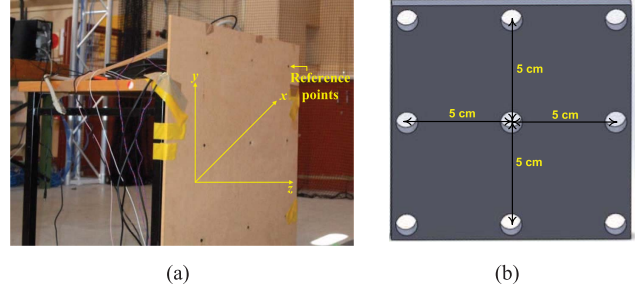


Fig. 9. Experimental setup: (a) configuration of reference plane and (b) targets.

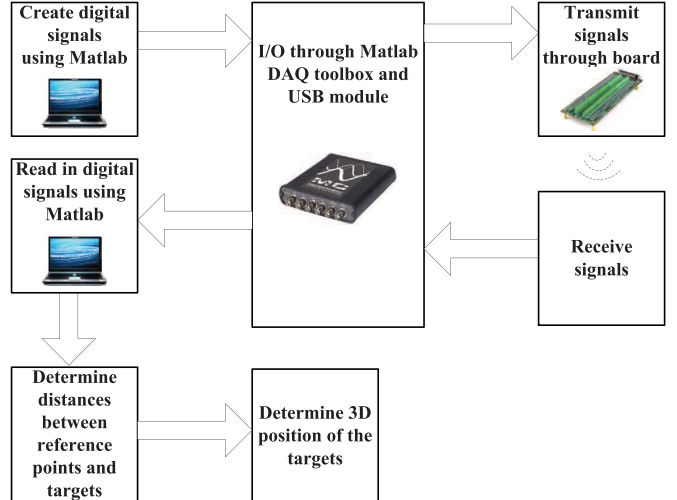


Fig. 10. Illustration of the experimental procedure

that was created using a 3D printer) approximately 1200 mm away from the reference points and the gap between them was 5 cm with a precision of 0.3 mm (as shown in Fig. 9(b)).

The configuration of the reference points and targets are shown in Fig. 9(a) and Fig. 9(b) respectively. In Fig. 9(a) although 9 transmitters (reference points) are visible, only the side ones in the middle row and central one in the top row were used and in Fig. 9(b) although 9 holes (where the transmitters were placed) are visible, the right one in the top row was not used. Piezotite MA40S4S and MA40S4R US devices, with a center frequency of 40 kHz, were used as transmitters and receivers respectively. According to the procedure described in Section III, with a sampling rate of 1 Msample/s,

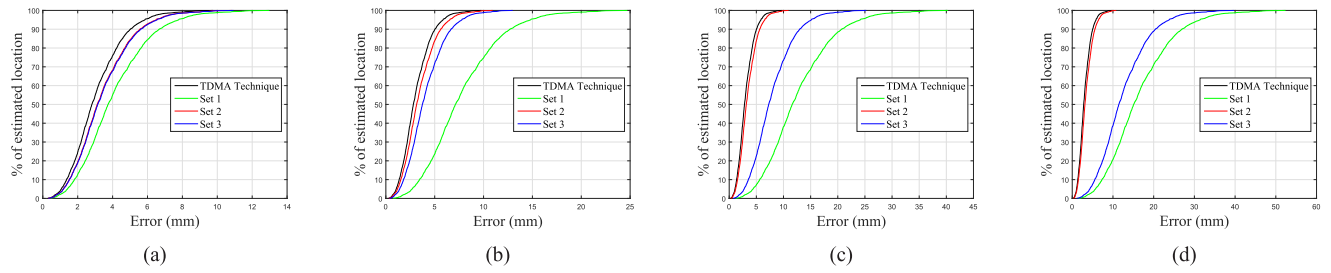


Fig. 11. Cumulative absolute location errors (from experiments) for TDM technique and all sets of pseudo-orthogonal chirp waveforms when number of targets were: (a) 2; (b) 4; (c) 6; and (d) 8

TABLE III
ABSOLUTE LOCATION ERRORS (FROM EXPERIMENTS) OF TARGET OBTAINED FOR TDM TECHNIQUE AND ALL SETS OF PSEUDO-ORTHOGONAL CHIRP WAVEFORMS IN TERMS OF CDF AND RMSE (mm)

Methods	Number of Transmitters							
	2		4		6		8	
	RMSE	CDF	RMSE	CDF	RMSE	CDF	RMSE	CDF
TDM	3.4132	5.0202	3.4166	5.0252	3.4132	5.0202	3.4090	5.0141
Set 1	4.5398	6.6773	8.6438	12.7135	14.0916	20.7262	18.3227	26.9494
Set 2	3.7870	5.5700	3.8210	5.6200	3.8210	5.6200	3.7794	5.5588

three sets of pseudo-orthogonal chirps, were generated, from a 35-45 kHz/10 ms chirp signal. The waveforms contained in sets 1 to 3 were same as the number of transmitters. The waveforms contained in each set were transmitted simultaneously from the targets and received by the receivers.

The experimental process is shown in Fig. 10. The input signals to the transmitters were from a screw pin board [42] which was connected to a Measurement Computing USB-1604 data acquisition (DAQ) module (the sampling rate of which was 1 Msample/s) [42]. The DAQ was also connected to a laptop and hence Matlab, in order to be able to send the transmission signals. This configuration also allowed for the capture of the received signal using the DAQ and the DAQ toolboxes in Matlab. The setup was the same for every set of pseudo-orthogonal chirp waveforms and each location measurement was repeated 100 times. To demonstrate the performance of the proposed approaches, the positions of the targets (transmitters) were also calculated by the TDM technique using 35-45 kHz/10 ms chirp. As the sound velocity depends on temperature, to measure the room temperature a digital thermometer was used and the corresponding velocity was measured. The measured temperature (φ) was 23°C and its corresponding velocity (v) was calculated as 345.10 m/s using the formula $v = (331.3 + 0.6\varphi)$ m/s. Since the effect of humidity on the speed of sound is much smaller than for temperature, the effect of humidity on sound velocity was assumed to be negligible. Please note that as the measurements were taken over a short period of time, the effects of variations in temperature and humidity on the sound's velocity were assumed to be negligible. Therefore, the sound velocity was assumed to be constant during the experiments.

VII. RESULTS

The absolute location errors of the transmitters obtained from the experiments for each set of pseudo-orthogonal chirps

and TDM technique are shown in Fig. 11 in terms of CDF. For 90% of cases, the cumulative errors for the proposed and TDM approaches are summarized in Table III along with RMSEs. The computational complexity in terms of signal length for each set was same as simulation results shown in Fig. 7. The results show that, for the same environment, the errors for each set of orthogonal chirp waveforms and computational complexity varied depending on the cross-correlation suppression and signal repetition property respectively. The positioning error of the orthogonal chirp sets 1 and 2 were higher and lower as their cross-correlations suppressions were lower and higher respectively (that is, the MAI was higher and lower respectively). On the other hand, the computational complexity of the orthogonal chirp sets 1 and 2 were lower and higher as signal's repetition property was higher in set 2 whereas there was no signal repetition occurred in set 1. It has been noticed that for set 3 a satisfactory tradeoff between the computational cost (shown in Fig. 7) and positioning errors (shown in Fig. 11 and its corresponding Table III) is noticeable as it was generated by combining the underlying techniques of set 1 and set 2.

It can be observed that the experimental results (Fig. 11, Table III) are degraded when compared to the simulation results (Fig. 6, Table III). This is because the bandwidth restriction imposed by resonant transducers i.e., the transducers did not have enough bandwidth to transmit the assigned chirp signals. As it is well known that for a linear chirp the correlation width (Δc) is inversely proportional to the bandwidth (B) (i.e., $\Delta c \propto \pm \frac{1}{B}$), from the experimental data (for TDM technique) we compared the auto-correlation width of a transmitted and received linear chirp signal in Fig. 12 where we can see that although we transmitted a signal with 10 kHz bandwidth, we received the signal with a 6 kHz bandwidth (centre frequency was 40 kHz) which indicates the bandwidth restriction imposed by resonant transducers.

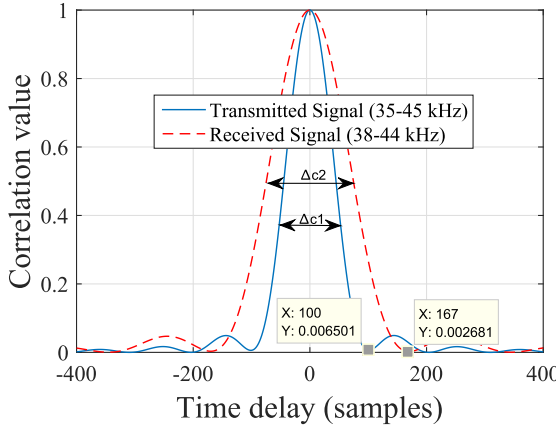


Fig. 12. Auto-correlation width of the transmitted and received signal where the correlation width (Δc_1) 100 and (Δc_2) 167 refers 10 kHz and 6 kHz respectively according to the formula $\Delta c \simeq \pm \frac{1}{T_s B}$ [41] where T_s is the sampling interval.

VIII. CONCLUSIONS AND FUTURE WORK

In this paper, to facilitate multiple-access transmission in a chirp-based UPS, we analyzed three sets (sets 1 to 3) of pseudo-orthogonal chirp waveforms which have the main advantage that, as multiple transmitters can simultaneously transmit these signals with significantly low interference, it is possible to exploit the full bandwidth for each waveform. Also, they have all the benefits of a classic chirp waveform. As, for simultaneous transmission, the all the approaches (i.e., sets 1 to 3) did not use the TDM technique, there was no impact on the system's update rate.

The performances of sets 1 to 3 of the pseudo-orthogonal chirps were experimentally validated for an active mobile architecture where the number of reference points and a maximum number of targets were three and eight respectively. The lowest and highest accuracy was obtained from set 1 and set 2 respectively. In set 1 that uses the diversity of the chirp rates for multiple-access, the location estimation error was proportional to the scalability i.e., when the number of transmitters was increasing the error in location estimation was also increasing. On the other hand, in set 2 that exploits the orthogonality of the sub-carriers of a chirp waveform for multiple-access, the computational complexity was proportional to the scalability i.e., when the number of transmitters was increasing the signal length was also increasing. As the waveforms in set 3 were generated by combining the underlying methodologies of sets 1 and 2 (i.e., it not only exploits the orthogonality of the sub-carriers of a chirp waveform but also chirp rates as a mechanism for assigning uniquely modulated chirp signals to transmitters), it provided a satisfactory tradeoff between the accuracy and computational cost.

It is worth noting that, although the performances of sets 1 to 3 of pseudo-orthogonal chirps were experimentally validated for US positioning, for large scale indoor positioning applications (e.g., human navigation, with the goal of directing users to their desired destinations on an active map, and robotic navigation with location sensors providing position information to a moving robot) near-far problem may be introduced if the transmitter is at a larger distance, or seen from a wider

angle, from the receiver, resulting in a lower relative amplitude and decorrelation caused by signal distortion with angle [13]. Therefore, our future work involves identifying the robustness of sets 1 to 3 of pseudo-orthogonal chirps to the near-far effect which can be achieved by employing successive interference cancellation algorithms described in [13], [43].

REFERENCES

- [1] A. J. Weiss and E. Weinstein, "Fundamental limitations in passive time-delay estimation—Part II: Wide-band systems," *IEEE Trans. Acoust. Speech Signal Process.*, vol. 31, no. 2, pp. 472–486, Feb. 1983.
- [2] N. B. Priyantha, A. Chakraborty, and H. Balakrishnan, "The cricket location-support system," in *Proc. 6th Annu. Int. Conf. Mobile Comput. Netw.*, 2000, pp. 32–43.
- [3] M. M. Saad, C. J. Bleakley, T. Ballal, and S. Dobson, "High-accuracy reference-free ultrasonic location estimation," *IEEE Trans. Instrum. Meas.*, vol. 61, no. 6, pp. 1561–1570, Jun. 2012.
- [4] M. Alloulah and M. Hazas, "An efficient CDMA core for indoor acoustic position sensing," in *Proc. Int. Conf. Indoor Positioning Indoor Navigat.*, 2010, pp. 1–5.
- [5] M. Hazas and A. Hopper, "Broadband ultrasonic location systems for improved indoor positioning," *IEEE Trans. Mobile Comput.*, vol. 5, no. 5, pp. 536–547, May 2006.
- [6] A. D. Angelis *et al.*, "Design and characterization of a portable ultrasonic indoor 3-D positioning system," *IEEE Trans. Instrum. Meas.*, vol. 64, no. 10, pp. 2616–2625, Oct. 2015.
- [7] L. Segers, D. V. Bavegem, A. D. Winne, S. Braeken, A. Touhafi, and K. Steenhaut, "An ultrasonic multiple-access ranging core based on frequency shift keying towards indoor localization," *Sensors*, vol. 15, no. 8, pp. 18641–18665, 2015.
- [8] L. Segers, J. Tiete, A. Braeken, and A. Touhafi, "Ultrasonic multiple-access ranging system using spread spectrum and MEMS technology for indoor localization," *Sensors*, vol. 14, no. 2, pp. 3172–3187, 2014.
- [9] S. J. Kim and B. K. Kim, "Accurate hybrid global self-localization algorithm for indoor mobile robots with two-dimensional isotropic ultrasonic receivers," *IEEE Trans. Instrum. Meas.*, vol. 60, no. 10, pp. 3391–3404, Oct. 2011.
- [10] U. Yayan, H. Yucel, and A. Yazici, "A low cost ultrasonic based positioning system for the indoor navigation of mobile robots," *J. Intell. Robot. Syst.*, vol. 78, nos. 3–4, pp. 541–552, Jun. 2015.
- [11] G. Ogris, T. Stiefmeier, H. Junker, P. Lukowicz, and G. Troster, "Using ultrasonic hand tracking to augment motion analysis based recognition of manipulative gestures," in *Proc. 9th IEEE Int. Symp. Wearable Comput.*, Sep. 2005, pp. 152–159.
- [12] R. Halmshaw, *Non-Destructive Testing*. London, U.K.: Edward Arnold, 1997.
- [13] F. Seco, J. C. Prieto, A. R. J. Ruiz, and J. Guevara, "Compensation of multiple access interference effects in CDMA-based acoustic positioning systems," *IEEE Trans. Instrum. Meas.*, vol. 63, no. 10, pp. 2368–2378, Oct. 2014.
- [14] A. Ward, A. Jones, and A. Hopper, "A new location technique for the active office," *IEEE Pers. Commun.*, vol. 4, no. 5, pp. 42–47, Oct. 1997.
- [15] M. Minami *et al.*, "DOLPHIN: A practical approach for implementing a fully distributed indoor ultrasonic positioning system," in *Proc. Int. Conf. Ubiquitous Comput.*, 2004, pp. 347–365.
- [16] J. A. Costa, N. Patwari, and A. O. Hero, III, "Distributed weighted-multidimensional scaling for node localization in sensor networks," *ACM Trans. Sensor Netw.*, vol. 2, no. 1, pp. 39–64, 2006.
- [17] H. Lim, L.-C. Kung, J. C. Hou, and H. Luo, "Zero-configuration indoor localization over IEEE 802.11 wireless infrastructure," *Wireless Netw.*, vol. 16, no. 2, pp. 405–420, Feb. 2010.
- [18] N. B. Priyantha, "The cricket indoor location system," Ph.D. dissertation, Dept. Elect. Eng. Comput. Sci., Massachusetts Inst. Technol., Cambridge, MA, USA, 2005.
- [19] R. Queiros, F. C. Alegria, P. S. Girao, and A. C. Serra, "Cross-correlation and sine-fitting techniques for high-resolution ultrasonic ranging," *IEEE Trans. Instrum. Meas.*, vol. 59, no. 12, pp. 3227–3236, Dec. 2010.
- [20] J. C. Jackson, R. Summan, G. I. Dobie, S. M. Whiteley, S. G. Pierce, and G. Hayward, "Time-of-flight measurement techniques for airborne ultrasonic ranging," *IEEE Trans. Ultrason., Ferroelect., Freq. Control*, vol. 60, no. 2, pp. 343–355, Feb. 2013.
- [21] H. Piontek, M. Seyffer, and J. Kaiser, "Improving the accuracy of ultrasound-Based localisation systems," *Pers. Ubiquitous Comput.*, vol. 11, no. 6, pp. 439–449, 2007.

- [22] H. Lee, T. H. Kim, J. W. Choi, and S. Choi, "Chirp signal-based aerial acoustic communication for smart devices," in *Proc. IEEE Conf. Comput. Commun. (INFOCOM)*, Apr. 2015, pp. 2407–2415.
- [23] J. Fürst, K. Chen, M. Aljarrah, and P. Bonnet, "Leveraging physical locality to integrate smart appliances in non-residential buildings with ultrasound and Bluetooth low energy," in *Proc. IEEE 1st Int. Conf. Internet-Things Design Implement. (IoTDI)*, Apr. 2016, pp. 199–210.
- [24] S. Saleemian, H. Keivani, and O. Mahdiyar, "Comparison of radar pulse compression techniques," in *Proc. IEEE Int. Symp. Microw., Antenna, Propag. EMC Technol. Wireless Commun.*, vol. 2, 2005, pp. 1076–1079.
- [25] P. R. Atkins, T. Collins, and K. G. Foote, "Transmit-signal design and processing strategies for sonar target phase measurement," *IEEE J. Sel. Topics Signal Process.*, vol. 1, no. 1, pp. 91–104, Jun. 2007.
- [26] S. I. Lopes, J. M. N. Vieira, and D. Albuquerque, "High accuracy 3D indoor positioning using broadband ultrasonic signals," in *Proc. 11th IEEE Int. Conf. Trust, Secur. Privacy Comput. Commun.*, Jun. 2012, pp. 2008–2014.
- [27] H. Schweinzer and M. Syafrudin, "LOSNU: An ultrasonic system enabling high accuracy and secure TDOA locating of numerous devices," in *Proc. Int. Conf. Indoor Positioning Indoor Navigat.*, 2010, pp. 1–8.
- [28] C. Randell and H. Muller, "Low cost indoor positioning system," in *Proc. Int. Conf. Ubiquitous Comput.*, 2001, pp. 42–48.
- [29] N. B. Priyantha, A. K. L. Miu, H. Balakrishnan, and S. Teller, "The cricket compass for context-aware mobile applications," in *Proc. 7th Annu. Int. Conf. Mobile Comput. Netw.*, 2001, pp. 1–14.
- [30] P. Lazik and A. Rowe, "Indoor pseudo-ranging of mobile devices using ultrasonic chirps," in *Proc. 10th ACM Conf. Embedded Netw. Sensor Syst.*, 2012, pp. 99–112.
- [31] A. Smith, H. Balakrishnan, M. Goraczko, and N. B. Priyantha, "Tracking moving devices with the cricket location system," in *Proc. 2nd Int. Conf. Mobile Syst. Appl. Services*, Jun. 2004, pp. 190–202.
- [32] R. Casas, D. Cuartielles, A. Marco, H. J. Gracia, and J. L. Falco, "Hidden issues in deploying an indoor location system," *IEEE Pervasive Comput.*, vol. 6, no. 2, pp. 62–69, Apr. 2007.
- [33] M. R. McCarthy, H. L. Muller, A. D. Calway, and R. E. Wilson, "Position and velocity recovery from independent ultrasonic beacons," in *Proc. 14th Eur. Signal Process. Conf.*, 2006, pp. 4–8.
- [34] A. Marco, R. Casas, J. Falco, H. Gracia, J. I. Artigas, and A. Roy, "Location-based services for elderly and disabled people," *Comput. Commun.*, vol. 31, no. 6, pp. 1055–1066, 2008.
- [35] M. O. Khyam, M. J. Alam, A. J. Lambert, C. R. Benson, and M. R. Pickering, "High precision ultrasonic positioning using phase correlation," in *Proc. 6th Int. Conf. Signal Process. Commun. Syst.*, 2012, pp. 1–6.
- [36] Y. Zejie, Y. Yanming, L. Qihang, and W. Wenlian, "A new system for three-Dimensional kinematic trajectory acquisition and analysis—I. The application of an ultrasonic technique to human gait analysis," *Med. Eng. Phys.*, vol. 18, no. 5, pp. 420–426, 1996.
- [37] M. Addlesee *et al.*, "Implementing a sentient computing system," *Computer*, vol. 34, no. 8, pp. 50–56, Aug. 2001.
- [38] H. Shen, S. Machineni, C. Gupta, and A. Papandreou-Suppappola, "Time-varying multichirp rate modulation for multiple access systems," *IEEE Signal Process. Lett.*, vol. 11, no. 5, pp. 497–500, May 2004.
- [39] J.-H. Kim, M. Younis, A. Moreira, and W. Wiesbeck, "Spaceborne MIMO synthetic aperture radar for multimodal operation," *IEEE Trans. Geosci. Remote Sens.*, vol. 53, no. 5, pp. 2453–2466, May 2015.
- [40] M. M. Saad, C. J. Bleakley, and S. Dobson, "Robust high-accuracy ultrasonic range measurement system," *IEEE Trans. Instrum. Meas.*, vol. 60, no. 10, pp. 3334–3341, Oct. 2011.
- [41] P. Misra, N. Kottele, B. Kusy, D. Ostry, and S. Jha, "Acoustical ranging techniques in embedded wireless sensor networked devices," *ACM Trans. Sensor Netw.*, vol. 10, no. 1, pp. 15:1–15:38, Dec. 2013.
- [42] *USB-1604HS-2AO DAQ Multifunction Synchronous Data Acquisition Board User's Guide*, accessed on Apr. 13, 2017. [Online]. Available: <http://www.mccdaq.com/PDFs/Manuals/USB-1604HS-2AO.pdf>
- [43] W. Q. Wang, "Large-area remote sensing in high-altitude high-speed platform using MIMO SAR," *IEEE J. Sel. Topics Appl. Earth Observ. Remote Sens.*, vol. 6, no. 5, pp. 2146–2158, Oct. 2013.



Mohammad Omar Khyam received the B.Sc. degree in electronics and telecommunication engineering from the Rajshahi University of Engineering and Technology, Rajshahi, Bangladesh, in 2010, and the Ph.D. degree from the University of New South Wales, Australia, in 2015. He is currently a Post-Doctoral Research Fellow with the National University of Singapore. His research interests include signal processing and wireless communication.



Shuzhi Sam Ge (S'90–M'92–SM'99–F'06) received the B.Sc. degree from the Beijing University of Aeronautics and Astronautics, Beijing, China, in 1986, and the Ph.D. degree from the Imperial College of Science, Technology and Medicine, University of London, London, U.K., in 1993. He is currently the Founding Director of the Robotics Institute and the Institute of Intelligent Systems and Information Technology, University of Electronic Science and Technology of China, Chengdu, China. He is also the Founding Director of the Social Robotics Laboratory, Interactive Digital Media Institute, National University of Singapore, Singapore, where he is a Professor with the Department of Electrical and Computer Engineering. He is the Editor-in-Chief of the *International Journal of Social Robotics*. He has served as an Associate Editor for a number of flagship journals. He has served as the Vice President of technical activities from 2009 to 2010, membership activities from 2011 to 2012, and the IEEE Control Systems Society.



Xinde Li (M'09–SM'16) received the Ph.D. degree in control theory and control engineering from the Department of Control Science and Engineering, Huazhong University of Science and Technology, Wuhan, China, in 2007. From 2012 to 2013, he was a Visiting Scholar with the School of Interactive Computing, Georgia Institute of Technology. He was a Post-Doctoral Research Fellow with the Department of Electrical and Computer Engineering, National University of Singapore, in 2016. He joined the School of Automation, Southeast University, Nanjing, China, where he is currently a Professor and a Ph.D. Supervisor. His research interests include information fusion, object recognition, computer vision, intelligent robot, and human–robot interaction. He received the Talent of Qing Lan Project Award of Jiangsu Province and a Six Major Top-Talent Plan Award of Jiangsu Province, China.



Mark R. Pickering (S'92–M'95) was born in Biloela, Australia, in 1966. He received the B.Eng. degree from the Capricornia Institute of Advanced Education, Rockhampton, Australia, in 1988, and the M.Eng. and Ph.D. degrees from the University of New South Wales, Canberra, Australia, in 1991 and 1995, respectively, all in electrical engineering. He was a Lecturer from 1996 to 1999 and a Senior Lecturer from 2000 to 2009 with the School of Electrical Engineering and Information Technology, the University of New South Wales, where he is currently an Associate Professor. His research interests include video and audio coding, medical imaging, data compression, information security, data networks, and error-resilient data transmission.